DALTON
FULL PAPER

Iron(I) complexes of 2,9-bis(2-hydroxyphenyl)-1,10-phenanthroline (H_2dophen) as electrocatalysts for carbon dioxide reduction. X-Ray crystal structures of $[Fe(dophen)Cl]_2 \cdot 2HCON(CH_3)_2$ and $[Fe(dophen)(N\text{-}MeIm)_2]ClO_4$ (N-MeIm = 1-methylimidazole) †

So-Ngan Pun,[a] Wan-Hung Chung,[a] Kin-Ming Lam,[a] Peng Guo,[a] Pak-Ho Chan,[a] Kwok-Yin Wong,*[a] Chi-Ming Che,*[b] Tai-Yuen Chen[c] and Shie-Ming Peng[c]

[a] *Department of Applied Biology and Chemical Technology, The Hong Kong Polytechnic University, Hunghom, Kowloon, Hong Kong, P.R. China. E-mail: bckywong@polyu.edu.hk*
[b] *Department of Chemistry, The University of Hong Kong, Pokfulam Road, Hong Kong, P.R. China*
[c] *Department of Chemistry, National Taiwan University, Taipei, Taiwan, ROC*

Received 18th September 2001, Accepted 21st November 2001
First published as an Advance Article on the web 31st January 2002

The crystal structure of two iron complexes of 2,9-bis(2-hydroxyphenyl)-1,10-phenanthroline (H_2dophen) $[Fe(dophen)Cl]_2 \cdot 2HCON(CH_3)_2$ [**1**·$2HCON(CH_3)_2$] and $[Fe(dophen)(N\text{-}MeIm)_2]ClO_4$ [**2**] (N-MeIm = 1-methylimidazole) have been determined: **1**·$2HCON(CH_3)_2$, monoclinic, space group $P2_1/n$, $a = 11.141(4)$, $b = 15.519(4)$, $c = 13.387(3)$ Å, $\beta = 93.76(2)°$, $Z = 4$; **2**, triclinic, space group $P\bar{1}$, $a = 10.293(1)$, $b = 12.395(3)$, $c = 12.400(6)$ Å, $\alpha = 105.04(4)$, $\beta = 90.54(4)$, $\gamma = 99.93(1)°$, $Z = 2$. The cyclic voltammograms of **1** and **2** in dimethylformamide show that the iron complexes undergo three successive reversible reductions with $E_{1/2} = -0.80$ V, -2.02 V, -2.45 V for **1** and -0.75 V, -2.03 V and -2.45 V for **2** *vs.* the ferrocenium/ferrocene couple ($Cp_2Fe^{+/0}$) respectively. The first two couples are assigned as the Fe(III)/Fe(II) and Fe(II)/Fe(I) couples, whereas the couple at -2.45 V is assigned to the reduction of the dophen ligand. The Fe(I) species are active towards CO_2 reduction. Electrolysis of CO_2 in the presence of **1** or **2** at -2.0 V *vs.* $Cp_2Fe^{+/0}$ gave a mixture of carbon monoxide, formate and oxalate, with formate being the major product. The rate of CO_2 reduction was enhanced by the addition of 1,1,1-trifluoroethanol or methanol as the proton source to the electrolyte. Iron carbonyl and iron formato species were detected as intermediates by *in-situ* FTIR spectroelectrochemistry.

Introduction

The concentration of carbon dioxide in the atmosphere has been increasing steadily since the beginning of industrialization, from ~280 parts per million by volume (ppmv) to its present value of ~368 ppmv.[1] Electrochemical reduction of CO_2 to carbon-based fuels using renewable energy sources such as solar electricity is an appealing means of recycling this greenhouse gas.[2–5] Direct electroreduction of carbon dioxide in an aprotic medium occurs at a very negative potential (*ca.* -2.2 V *vs.* SCE) and leads to the formation of the high energy $CO_2^{\bullet-}$ intermediate.[6] In the presence of a suitable proton source, however, the reduction of carbon dioxide should be able to take place at moderately negative potentials. For example, the thermodynamic potential for the reduction of carbon dioxide to carbon monoxide and formate in pH 7 aqueous solution are -0.52 and -0.61 V *vs.* NHE respectively.[6] A number of transition metal complexes including metalloporphyrins,[7] Pd phosphine,[8] Ni and Co tetraaza-macrocycles,[9] and Ru[10] and Re[11] polypyridyl complexes are effective homogeneous catalysts in the electrochemical reduction of carbon dioxide. In most cases, the reduction products are carbon monoxide and/or formate.

In view of the increasingly stringent environmental rules on the chemical industries, there is a compelling need to develop catalysts that are non-toxic and inexpensive. Iron catalysts are obvious choices in this aspect. Iron complexes of tetraphenylporphyrin,[12] porphycene,[13] chromotropic acid[14] and terpyridine[15] have been reported to catalyze the electrochemical reduction of carbon dioxide. Amongst these, iron(0) porphyrin[12] stands out to be an effective and selective catalyst in the conversion of CO_2 to CO. Therefore, it would be interesting to investigate the catalytic properties of its analogues with tetradentate, non-porphyrin ligands. Although iron Schiff base [Fe(salen), H_2salen = *N,N′*-bis(salicylidene)ethylenediamine] appears to be a candidate, the ease of hydrolysis of the imino group in the salen ligand limits its applications.[16] The ligands 6,6′-bis(2-hydroxyphenyl)-2,2′-bipyridine (H_2dobpy) and 2,9-bis(2-hydroxyphenyl)-1,10-phenanthroline (H_2dophen), being structurally similar to H_2salen but with no free imino bonds, should allow the preparation of robust metal catalysts.[16,17] Therefore we have conducted an investigation on iron complexes of H_2dophen as electrocatalysts for CO_2 reduction. Experiments were conducted in the presence of various proton sources to investigate their effect on the selectivity of the reaction.

Experimental

Materials

2,9-Bis(2-hydroxyphenyl)-1,10-phenanthroline (H_2dophen) was synthesized as reported in the literature.[16,18] Anhydrous iron(III) chloride was obtained from Janssen Chemical Co. Dimethyl

† Electronic supplementary information (ESI) available: plots of $E_{1/2}$ *vs.* log [N-MeIm] for couples I and II in the UV-visible thin layer spectrum of **2** (S1) and $^{13}CO_2$ isotope experiments of **2** (S2). See http://www.rsc.org/suppdata/dt/b1/b108472k/

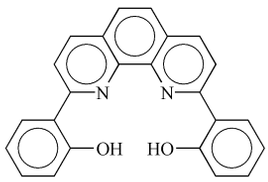

H_2dophen

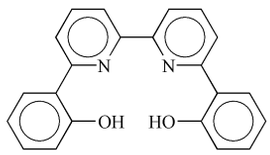

H_2dobpy

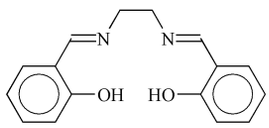

H_2salen

sulfoxide (DMSO) and dimethyl formamide (DMF) were distilled over anhydrous calcium sulfate under reduced pressure and stored over 4 Å molecular sieves. Tetra-*n*-butylammonium hexafluorophosphate (Aldrich) was recrystallized in ethanol and dried *in vacuo* at 80 °C for 24 h before used. Carbon dioxide (purity > 99.9%) was obtained from Hong Kong Oxygen Co. Other reagents obtained from Aldrich Chemical Co. were used as received.

Synthesis of iron complexes

$[Fe^{III}(dophen)Cl]_2 \cdot 2HCON(CH_3)_2$ [1·2HCON(CH$_3$)$_2$]. Anhydrous $FeCl_3$ (0.1 g) was added to a solution of H_2dophen in methanol (0.15 g in 50 mL). The colour of the mixture changed rapidly from pale yellow to dark green. Upon standing at room temperature, some dark green microcrystals precipitated out slowly. The dark green microcrystalline solid was filtered and washed with methanol (yield ~70%). Anal. For [Fe(dophen)Cl]CH_3OH. Calcd.: C, 61.82; H, 3.74; N, 5.77%. Found C, 61.17; H, 3.45; N, 5.78%. UV/VIS in DMF [λ_{max}/nm (ε/dm^3 mol^{-1} cm^{-1})]: 402 (11400), 314 (27500), μ_{eff} (solid) = 5.3 μ_B at room temperature. Crystals of **1**·2HCON(CH$_3$)$_2$ suitable for X-ray structural analysis were obtained by dissolving the dark green solid in dimethylformamide followed by vapour diffusion of diethyl ether to the solution.

$[Fe^{III}(dophen)(N\text{-}MeIm)_2]ClO_4$ [2] (N-MeIm = 1-methylimidazole). A mixture of 1-methylimidazole (0.12 g) and $[Fe(dophen)Cl]_2$ (0.15 g) in methanol (30 mL) was heated to *ca.* 60 °C for 15 min. The resulting solution was concentrated to *ca.* 15 mL by evaporation; excess $LiClO_4$ was added to precipitate the iron complex. A dark green solid of **2** appeared upon cooling the mixture at 5 °C in a refrigerator. The crude product was collected by filtration, and further purified by recrystallization in methanol–diethyl ether (Yield ~80%). Anal. for [Fe(dophen)-(N-MeIm)$_2$]ClO_4, Calcd.: C, 56.35; H, 3.82; N, 12.33%. Found: C, 56.28; H, 3.68; N, 12.26%. UV/VIS in CH_3CN [λ_{max}/nm (ε/cm^3 mol^{-1} cm^{-1})]: 396 (7900), 312 sh (21400), 282 (29500), 262 (29500), μ_{eff} (solid) = 5.99μ_B at room temperature. Crystals of **2** suitable for X-ray structural analysis were obtained by vapour diffusion of diethyl ether into a dimethylformamide solution of the complex.

Physical measurements

UV-visible spectra were recorded on a Milton Roy Spectronic 3000 diode array spectrophotometer. Magnetic susceptibility was measured by the Gouy method with mercury tetrathiocyanatocobaltate(III) as the calibrant. A Bioanalytical Systems (BAS) model 100W electrochemical analyzer was used in all electrochemical measurements. Tetra-*n*-butylammonium hexafluorophosphate (TBAH) was used as the supporting electrolyte unless otherwise stated. Cyclic voltammetry was performed in a conventional two-compartment electrochemical cell. The glassy carbon electrode was treated by polishing with 0.05 μm alumina on a microcloth and then sonicated for 5 min in deionized water followed by rinsing with the solvent used in the electrochemical studies. An $Ag/AgNO_3$ (0.1 M) electrode was used as reference electrode. The $E_{1/2}$ values are the average of the cathodic and anodic peak potentials for the oxidative and reductive waves. The $E_{1/2}$ of the ferrocenium/ferrocene couple ($Cp_2Fe^{+/0}$) was used as internal reference and all the potentials reported are quoted with respect to $Cp_2Fe^{+/0}$ ($E_{1/2}$ of $Cp_2Fe^{+/0}$ = +0.307 V *vs.* SCE[19]). Thin layer UV-visible spectroelectrochemistry was performed with a thin layer quartz cell of pathlength 0.5 mm, a platinum gauze working electrode, a platinum wire counter electrode and an $Ag/AgNO_3$ (0.1 M) reference electrode. The electrolyte was thoroughly degassed with pre-purified argon gas before each measurement.

In-situ FTIR spectroelectrochemical studies were performed on a Nicolet Avatar 360 FTIR spectrometer in the reflectance mode with a wide band mercury cadmium telluride (MCT) detector. The cell was a standard three-electrode thin layer cell[20,21] with a CaF_2 window, a platinum foil counter electrode, a glassy carbon working electrode (o.d. = 6 mm) and an $Ag/AgNO_3$ (0.1 M) reference electrode. The potential of the spectroelectrochemical cell was controlled by a Princeton Applied Research model 362 potentiostat. The FTIR spectrometer was equipped with a Spectra-Tech Series 500 variable angle specular reflectance accessory which allowed the spectral reflectance measurement to be carried out at incident angles in the range 30–80°; the optimum angle for maximum reflectance was determined before each experiment and was usually around 55°. The distance between the working electrode and the CaF_2 window was adjusted to accommodate a thin layer of electrolyte (*ca.* 1 mm thick) for spectroelectrochemical measurement. A reference potential was chosen (E_1) at which a reference spectrum S_1 was collected and subsequent spectra, S_2, were collected at successive potentials (E_2). Each IR spectrum was recorded as a difference spectrum $\Delta R/R$, where R is the reflectance and ΔR is the difference in reflectance between S_2 and S_1. It follows that both positive and negative peaks can appear in the difference spectrum: a positive peak ($+\Delta R/R$) represents absorption from species that decrease in concentration in the thin layer on stepping the potential from E_1 to E_2. A negative peak ($-\Delta R/R$) represents a gain in the concentration of that particular species in the thin layer. All the spectra were collected at 8 cm^{-1} resolution and consist of 100 co-added and averaged scans. The sample compartment of the FTIR spectrometer was purged by N_2 prior to the spectroelectrochemical measurements to ensure the removal of CO_2 and water vapour.

Constant potential electrolysis was performed in a gas-tight three-compartment cell. Reticulated vitreous carbon obtained from the Electrosynthesis Co. was used as the working electrode. A control experiment was always performed by electrolysing a blank solution saturated with N_2. When an electrolysis had been completed, gas samples were taken from the head-space above the solution in the working electrode compartment and analyzed for CO and H_2 by a Hewlett-Parkard model 5890 gas chromatograph equipped with a thermal conductivity detector. A stainless steel column (6 ft × 1/8 in) packed with 5 Å molecular sieves was employed in the analysis; helium was used as the carrier gas. Formate and oxalate ions in the solution were analyzed by a Waters Associate model 510 liquid chromatograph with a Supelcogel C-610H column : A 10 mL aliquot of the electrolyte was taken; the solvent (DMSO or DMF) was removed from the sample by evaporation under reduced pressure. Distilled water (20 mL) was added to the residue to precipitate out the TBAH supporting electrolyte. Analysis for formate and oxalate were conducted on the aqueous filtrate after removal of TBAH by filtration.

X-Ray structural analysis

The crystal data and details of collection and refinement of

Table 1 Crystal data for $[Fe(dophen)Cl]_2 \cdot 2HCON(CH_3)_2$ [**1**·2HCON$(CH_3)_2$] and $[Fe(dophen)(N\text{-}MeIm)_2]ClO_4$ [**2**]

Complex	**1**·2HCON$(CH_3)_2$	**2**
Formula	$FeC_{24}H_{21}N_2O_2Cl \cdot C_3H_7NO$	$FeC_{32}H_{26}N_6O_6Cl$
M_r	533.92	681.99
Crystal dimensions mm	0.30 × 0.40 × 0.40	0.3 × 0.3 × 0.25
Crystal system	Monoclinic	Triclinic
Space group	$P2_1/n$	$P\bar{1}$
a/Å	11.141(4)	10.293(1)
b/Å	15.519(4)	12.395(3)
c/Å	13.387(3)	12.400(6)
α/°	—	105.04(4)
β/°	93.76(2)	90.54(4)
γ/°	—	99.93(1)
U/Å^3	2310(1)	1502.5(8)
λ Å	0.70930	0.71070
F(000)	1112	702
Z	4	2
D_c/g cm^{-3}	1.536	1.507
Scan mode	θ–2θ	θ–2θ
No. of reflections in unit cell determination	24	24
2θ range	19.10–22.62°	18.86–27.50°
μ(Mo-K$_\alpha$)/mm^{-1}	0.80	0.65
F(000)	1112	702
No. unique reflections	4051	3915
No observed reflections ($\|I_o\| > 2\sigma\|I_o\|$)	2753	3109
R	0.041	0.057
R_w	0.033	0.042
GOF	2.05	3.69
Residual electron density/e Å^{-3}	0.49 to −0.37	0.88 to −0.65

[a] $R = \Sigma\big|\,|F_o| - |F_c|\,\big|/\Sigma|F_o|$. $R_w = [\Sigma w(|F_o| - |F_c|)^2/\Sigma w|F_o|^2]^{1/2}$. GOF $= [\Sigma w(|F_o| - |F_c|)^2/(n-p)]^{1/2}$.

1·2HCON$(CH_3)_2$ and **2** are summarized in Table 1. Intensities were measured on a Nonius CAD4 diffractometer using the θ–2θ scan mode ($2\theta_{max}$ = 50° for **1**·2HCON$(CH_3)_2$ and 45° for **2**; scan speed 2.35–8.24° min^{-1}). Graphite-monochromated Mo-Kα radiation was used throughout. The structures were solved by the Patterson method and refined by least squares using an NRCC-SDP-VAX software package.[22] The last least-squares cycle was calculated with 56 atoms, 317 parameters and 2753 reflections ($|I_o| > 2\sigma|I_o|$) out of 4051 unique reflections for **1**·2HCON$(CH_3)_2$ and with 72 atoms, 416 parameters and 3109 reflections ($|I_o| > 2\sigma|I_o|$) out of 3915 unique reflections for **2**. Selected bond distances and angles for **1**·2HCON$(CH_3)_2$ and **2** are given in Tables 2 and 3 respectively.

CCDC reference numbers 155477 and 155478.

Results and discussion

Fig. 1 shows a perspective view of $[Fe(dophen)Cl]_2$. The complex exists as a dimer consisting of two non-symmetric FeN_2O_3Cl units bridged by two oxygen atoms of the phenolate ligands. The structure is similar to that of $[Fe(salen)Cl]_2$.[23] The Fe–Fe′ and Fe′–O (bridging oxygen) distances are 3.367(1) and 2.313(3) Å respectively. The Fe–O(1), Fe–O(2), Fe–N(1) and Fe–N(2) distances of 1.863(3), 1.937(2), 2.124(3) and 2.113(3) Å respectively are close to the related values in $[Fe(salen)Cl]_2$ (Fe–O 1.898(9)–1.978(7) Å, Fe–N 2.098(9)–2.091(19) Å).

Fig. 2 shows a perspective view of the $[Fe(dophen)(N\text{-}MeIm)_2]^+$ cation. The Fe atom is surrounded by the equatorial dophen ligand with the two 1-methylimidazole ligands occupying the axial positions. The respective Fe–O and Fe–N (α-diimine) distances of 1.867(4)–1.877(4) Å and 2.122(5)–2.131(4) Å are close to those (1.863(3)–1.937(2) Å and 2.113(3)–2.124(3) Å) of **1**·2HCON$(CH_3)_2$. The Fe–N (α-diimine) bond distances are longer than the Fe–N bond distances of 1.967(8)–1.980(8) Å in the low spin $[Fe(phen)_3](ClO_4)_3 \cdot H_2O$.[24] The Fe–N (imidazole) bond distance of 2.153(5) Å is also longer that those (1.975(4)–1.976(4) Å) in the low spin $[Fe(bpc)(N\text{-}MeIm)_2]ClO_4$ complex (H_2bpc = 4,5-dichloro-1,2-bis(pyridinecarboxamido)benzene).[25]

Table 2 Selected bond distances (Å) and angles (°) for $[Fe(dophen)Cl]_2 \cdot 2HCON(CH_3)_2$

Fe–Cl	2.278(1)	O(1)–C(1)	1.318(4)
Fe–O(1)	1.863(3)	O(2)–C(22)	1.355(4)
Fe–O(2)	1.937(2)	N(1)–C(7)	1.343(5)
Fe′–O(2)	2.313(3)	N(1)–C(23)	1.360(5)
Fe–N(1)	2.124(3)	N(2)–C(16)	1.338(5)
Fe–N(2)	2.113(3)	N(2)–C(24)	1.360(5)
Fe–Fe′	3.367(1)		
Fe–O(2)–Fe′	104.4(1)	Cl–Fe–O(1)	97.94(9)
Fe–O(1)–C(1)	133.23(24)	Cl–Fe–O(2)	101.85(8)
Fe–O(2)–C(22)	120.17(22)	Cl–Fe–O(2)′	176.01(7)
Fe′–O(2)–C(22)	118.74(22)	Cl–Fe–N(1)	99.47(9)
Fe–N(1)–C(7)	126.8(3)	Cl–Fe–N(2)	91.85(9)
Fe–N(1)–C(23)	112.42(23)	O(1)–Fe–O(2)	104.63(11)
Fe–N(2)–C(16)	126.4(3)	O(1)–Fe–O(2)′	85.74(10)
Fe–N(2)–C(24)	113.66(24)	O(1)–Fe–N(1)	87.82(11)
Fe′–Fe–C(1)	143.48(4)	O(1)–Fe–N(2)	164.49(12)
Fe′–Fe–O(1)	95.41(8)	O(2)–Fe–O(2)′	75.59(10)
Fe′–Fe–O(2)	41.72(8)	O(2)–Fe–N(1)	153.43(12)
Fe′–Fe–O(2)′	33.87(6)	O(2)–Fe–N(2)	84.95(11)
Fe′–Fe–N(1)	114.91(9)	O(2)′–Fe–N(1)	82.18(10)
Fe′–Fe–N(2)	83.58(9)	O(2)′–Fe–N(2)	84.89(11)
N(1)–Fe–N(2)	78.68(12)		

Table 3 Selected bond distances (Å) and angles (°) for $[Fe(dophen)(N\text{-}MeIm)_2]ClO_4$

Fe–O(1)	1.867(4)	Fe–O(2)	1.877(4)
Fe–N(1)	2.131(4)	Fe–N(2)	2.122(5)
Fe–N(3) or Fe–N(5)	2.153(5)		
O(1)–C(11)	1.322(7)	O(2)–C(21)	1.317(7)
N(1)–C(1)	1.348(8)	N(1)–C(17)	1.347(8)
N(2)–C(2)	1.364(7)	N(2)–C(27)	1.356(7)
O(1)–Fe–O(2)	102.7(2)	O(1)–Fe–N(1)	88.6(2)
O(1)–Fe–N(2)	168.2(2)	O(1)–Fe–N(3)	92.6(2)
O(2)–Fe–N(1)	168.6(2)	O(2)–Fe–N(2)	89.1(2)
O(2)–Fe–N(3)	92.2(2)	N(1)–Fe–N(2)	79.6(2)
N(1)–Fe–N(3)	86.9(2)	N(2)–Fe–N(3)	87.0(2)
Fe–O(1)–C(11)	134.0(4)	Fe–O(2)–C(21)	133.6(4)
Fe–N(1)–C(1)	111.7(4)	Fe–N(1)–C(17)	126.8(4)
Fe–N(2)–C(2)	111.9(4)	Fe–N(2)–C(27)	126.5(4)
Fe–N(3)–C(3)	122.4(4)	Fe–N(3)–C(4)	132.2(4)

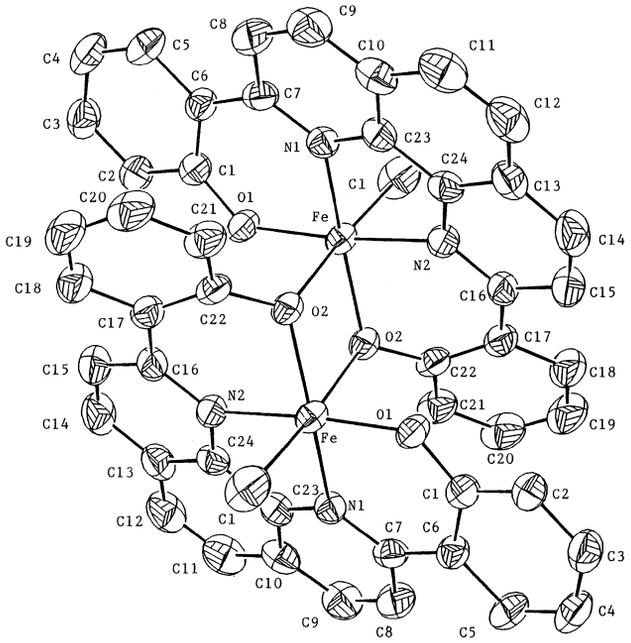

Fig. 1 An ORTEP plot of $[Fe(dophen)Cl]_2$ with atom numbering.

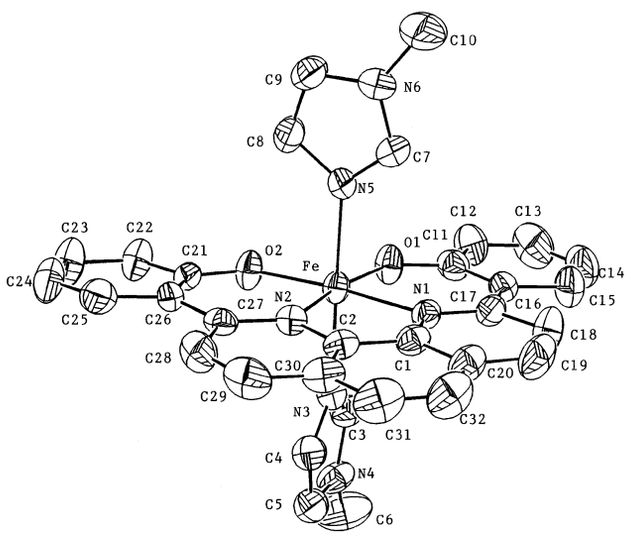

Fig. 2 An ORTEP plot of $[Fe(dophen)(N\text{-}Melm)_2]^+$ with atom numbering.

Electrochemical behavior of the complexes

As the iron complexes are only soluble in polar solvents such as DMF and DMSO, investigations on the electrochemistry of these complexes were conducted in these solvents. The voltammetric behavior of both complexes in DMSO and DMF are very similar. The cyclic voltammograms of **2** in DMF are shown in Fig. 3. Upon reductive scan, three reversible couples of similar size appear at $E_{1/2} = -0.75$, -2.03 and -2.45 V *vs.* $Cp_2Fe^{+/0}$ which are labeled couple I, II and III respectively ($E_{1/2} = -0.74$, -2.02 and -2.40 V *vs.* $Cp_2Fe^{+/0}$ in DMSO). The peak current of these couples is proportional to the square root of the scan rate (5–500 mV s^{-1}), which indicates that these redox processes are diffusion-controlled. The peak-to-peak separation (ΔE_p) of couples I–III are in the range of 60–80 mV, which is characteristic of reversible one-electron couples. Constant potential coulometry at -1.3 V and -2.3 V confirmed that both couple I and II are one-electron redox processes. Attempts to establish the stoichiometry of couple III by constant potential coulometry at -2.50 V, however, did not result in the decay of the current to background level. As these three couples have similar size and the ΔE_p of couple III is indicative

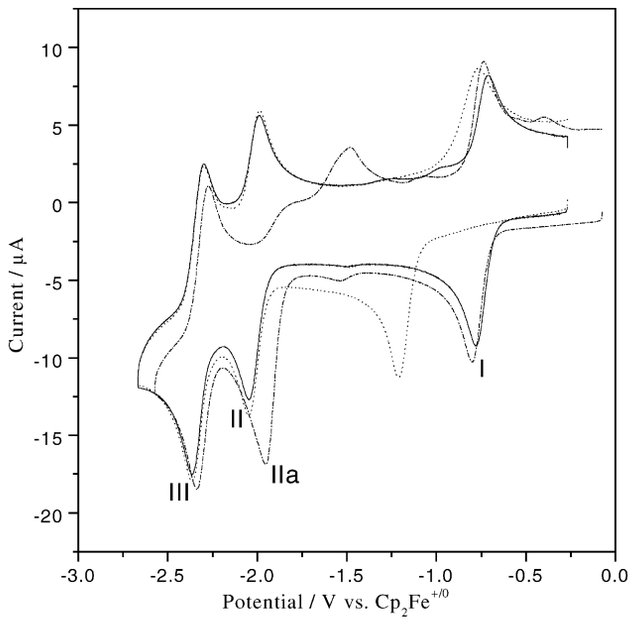

Fig. 3 Cyclic voltammograms of 0.3 mM **2** under 1 atm argon (—); in the presence of 3.0 mM diethylamine (· · ·) and under 1 atm CO (·–·–·) in dimethylformamide. Supporting electrolyte: 0.1 M TBAH. Working electrode: glassy carbon (0.2 cm^2). Scan rate: 100 mV s^{-1}.

of a one-electron process, it is reasonable to assign couple III as a one-electron couple.

Couple I is a metal-based Fe(III)/Fe(II) reduction as the free H_2dophen ligand is only reduced at a much more negative potential (-2.05 V). This assignment is supported by the observation that addition of excess Lewis base diethylamine to the electrolyte causes a significant shift in the $E_{1/2}$ and an increase in peak-to-peak separation of couple I (Fig. 3). As both the $E_{1/2}$ of couple II and III are very close to the reduction potential of H_2dophen, it is difficult to assign couple II and III as metal-or ligand-based processes. However, in the presence of CO, a significant shift in the $E_{1/2}$ of couple II is observed (Fig. 3). As CO is a strong π-acid ligand, our observation is consistent with the ligation of CO to the Fe^{II} center[26] and cathodic wave IIa can be assigned to the reduction of an Fe^{II}–CO species. The $E_{1/2}$ of couple III remains unchanged in the presence of hard or soft Lewis bases. These results support the assignments of couple I and II to metal-based redox processes and couple III to a ligand-based redox reaction.

In order to gain more insight into the nature of these redox processes, the spectral change accompanying each reduction step was monitored by *in-situ* UV-visible thin layer spectroelectrochemistry. The UV-visible spectrum of **2** shows an intense band at 396 nm which is also present in the spectrum of the free H_2dophen ligand. This band is therefore assigned to an electronic transition within the dophen ligand. Reduction of the H_2dophen ligand at -2.05 V results in a significant decrease in the intensity of this absorption band accompanied by a red shift of the peak maximum by over 60 nm. We would expect a similar spectral change to occur if the reduction of the iron complex is primarily a ligand-based process. Stepping the potential of the iron complex from -0.7 V to -1.75 V causes a slight shift of this absorption peak from 396 nm to 402 nm accompanied by a small increase in the absorption intensity (Fig. 4). This is in line with the assignment of couple I to a metal-based process; the small change in absorption peak maximum and intensity can be rationalized by a perturbation of the intraligand transition when the oxidization state of the metal center is changed. Stepping the potential from -1.75 V to -2.2 V only causes a small decrease in the intensity of this intraligand transition band. This indicates that couple II is unlikely to be a ligand-based reduction process. Further reduction of the complex by stepping the potential to -2.52 V,

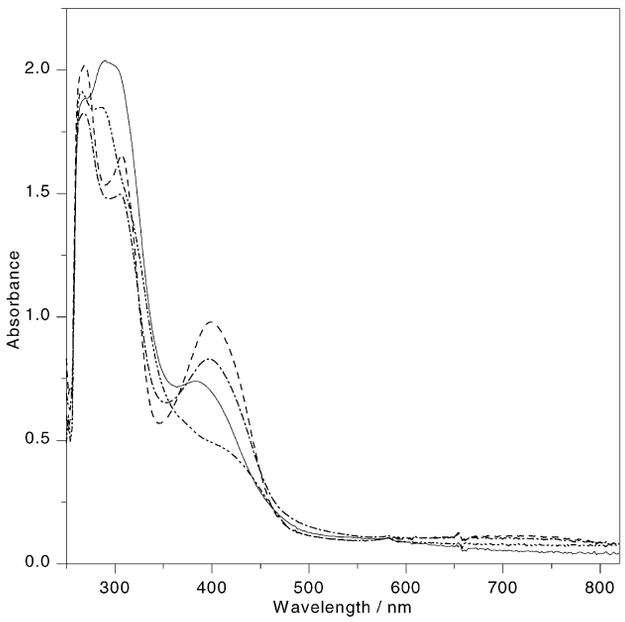

Fig. 4 The reduction of **2** in dimethylformamide as monitored by thin layer UV-visible spectroelectrochemistry. Spectrum of **2** (—); after electrolysis at −1.75 V (- - -); after electrolysis at −2.2 V (•–•–•) and after electrolysis at −2.52 V (–••–••–••) *vs.* $CpFe^{+/0}$.

however, causes a significant decrease in the intensity of the intraligand transition with a new hump that arises at around 440 nm. The spectral change accompanying the reduction of the iron complex at this potential is similar to that of the H_2dophen ligand, suggesting that couple III is primarily a ligand-based reduction. Therefore, couples II and III are assigned to the reduction of Fe(II) to Fe(I) and the reduction of $[Fe^{I}(dophen)]^{-}$ to $[Fe^{I}(dophen)^{\bullet}]^{2-}$ respectively.

The $E_{1/2}$ of couple I and II are dependent on the concentration of 1-methylimadizole in the electrolyte. Increasing the concentration of 1-methylimadazole causes a cathodic shift of both couples I and II. This is in contrary to the $E_{1/2}$ of couple III, which remains unchanged as the concentration of 1-methylimidazole is varied. The plots of $E_{1/2}$ *versus* log[N-MeIm] for both couples I and II are straight lines with slope equal to −55 mV (Fig. S1 in the supplementary information). The observation is consistent with the loss of one 1-methylimadizole ligand in each reduction step (eqn. 1–3):[27]

$$\text{Couple I: } [Fe^{III}(dophen)(N\text{-}MeIm)_2]^{+} + e^{-} \rightleftharpoons [Fe^{II}(dophen)(N\text{-}MeIm)] + N\text{-}MeIm \quad (1)$$

$$\text{Couple II: } [Fe^{II}(dophen)(N\text{-}MeIm)] + e^{-} \rightleftharpoons [Fe^{I}(dophen)]^{-} + N\text{-}MeIm \quad (2)$$

$$\text{Couple III: } [Fe^{I}(dophen)]^{-} + e^{-} \rightleftharpoons [Fe^{I}(dophen)^{\bullet}]^{2-} \quad (3)$$

Solutions of **1** in DMF and DMSO are non-conducting, indicating that the chloride ligand does not dissociate from the complex in solution. It is known from previous studies that the analogous complex $[Fe(salen)Cl]_2$ exists as a dimer in the solid state but a monomer in solution.[23,28] Complex **1** is expected to behave similarly in solution; *i.e.* it exists either as the five-coordinated [Fe(dophen)Cl] monomer or the six-coordinated [Fe(dophen)(Cl)(S)] complex with the sixth coordination position occupied by a solvent molecule S. The cyclic voltammogram of [Fe(dophen)Cl] in DMSO (Fig. 5) shows three reversible couples with $E_{1/2} = -0.78$ V, −2.06 V and −2.40 V *vs.* $Cp_2Fe^{+/0}$ (labeled I′, II′ and III′) respectively; in DMF, the $E_{1/2}$ of these three couples are −0.80 V, −2.02 V and −2.45 V *vs.* $Cp_2Fe^{+/0}$. The $E_{1/2}$ of couple I′ is dependent on the concentration of chloride in the electrolyte and a plot of $E_{1/2}$ *versus*

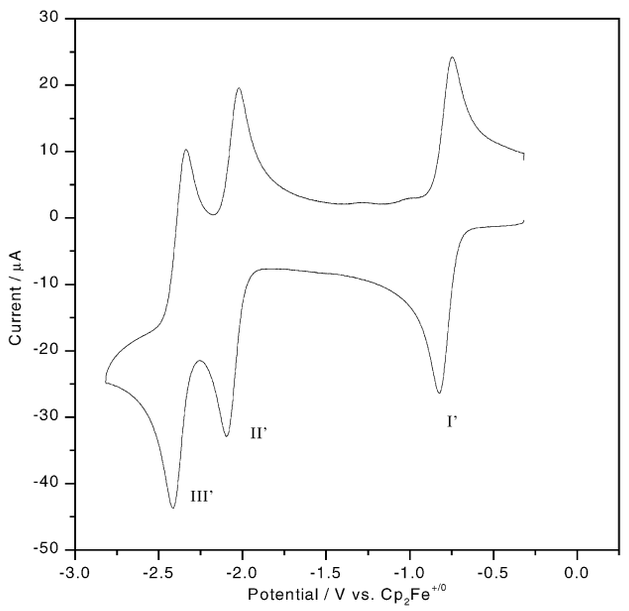

Fig. 5 Cyclic voltammograms of 0.5 mM **1** in dimethyl sulfoxide under 1 atm argon. Working electrode: glassy carbon (0.2 cm^2). Supporting electrolyte: 0.1 M TBAH. Scan rate: 100 mV s^{-1}.

log[Cl^-] gives a straight line with a slope of −55 mV. This is consistent with the loss of the chloride ligand upon the reduction of Fe(III) to Fe(II) (eqn. 4):

$$\text{Couple I}': [Fe^{III}(dophen)Cl] + e^{-} \rightleftharpoons [Fe^{II}(dophen)] + Cl^{-} \quad (4)$$

The $E_{1/2}$ of couples II′ and III′ are independent of [Cl^-] and these two couples can be assigned to the following reactions (5 and 6) accordingly:

$$\text{Couple II}': [Fe^{II}(dophen)] + e^{-} \rightleftharpoons [Fe^{I}(dophen)]^{-} \quad (5)$$

$$\text{Couple III}': [Fe^{I}(dophen)]^{-} + e^{-} \rightleftharpoons [Fe^{I}(dophen)^{\bullet}]^{2-} \quad (6)$$

At high [Cl^-] (> ten times concentration of the iron complex), the $E_{1/2}$ of couple II′ shifts cathodically with increase in [Cl^-]. This could be caused by the coordination of Cl^- to [Fe(dophen)Cl] to give $[Fe(dophen)Cl_2]^-$ at high chloride concentration, whereas the second chloride ligand is lost during the reduction of Fe(II) to Fe(I).

Electrocatalytic reduction of carbon dioxide

The cyclic voltammograms of **2** in DMSO under CO_2 atmosphere are shown in Fig. 6. In the presence of CO_2, the cathodic wave of the Fe(II)/Fe(I) couple is enhanced whereas the anodic wave is diminished. This indicates that the Fe(I) species is an active catalyst for CO_2 reduction. Under our experimental conditions, the catalytic current increases moderately when the scan rate is increased from 5 mV s^{-1} to 500 mV s^{-1}; hence the limiting condition that the catalytic current is independent of scan rate cannot be reached. Constant potential electrolysis at −2.0 V *vs.* $Cp_2Fe^{+/0}$ in DMSO or DMF resulted in the production of a mixture of carbon monoxide, formate and oxalate. No CO, $HCOO^-$ or $C_2O_4^{2-}$ could be detected in the control experiments without the iron complexes or in the absence of CO_2.

Although most molecular catalysts are known to produce a mixture of CO and $HCOO^-$ in CO_2 reduction, a number of catalyst systems are able to give either CO or $HCOO^-$ with high selectivity. In particular, the presence of a suitable proton source can improve the selectivity of the reaction. For example, addition of weak proton sources such as alcohol,[12b] water[11a] or

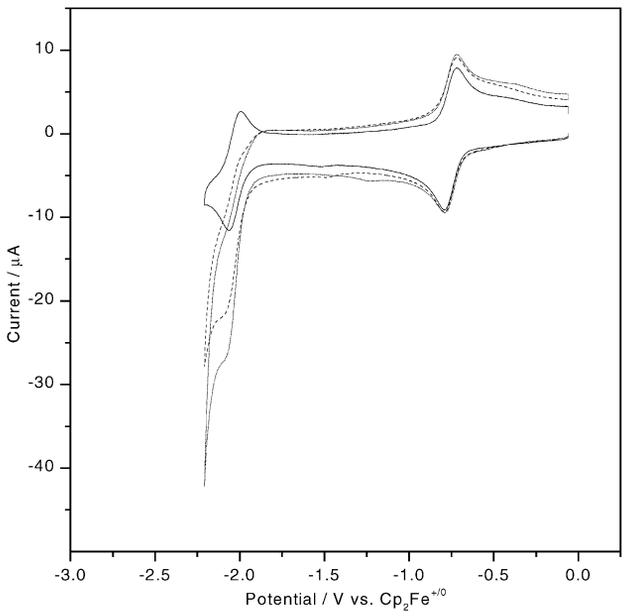

Fig. 6 Cyclic voltammograms of 0.4 mM **2** in dimethyl sulfoxide under 1 atm argon (—); under 1 atm CO_2 (- - -) and in the presence of 0.32 M CF_3CH_2OH under 1 atm CO_2 (· · ·) Working electrode: glassy carbon. Supporting electrolyte: 0.1 M TBAH. Scan rate: 100 mV s^{-1}.

fluoroboric acid[8b] to the electrolyte lead to the enhancement of reaction rate and selective formation of CO in some catalytic systems. Selective formation of $HCOO^-$ has been reported with protonated amine as the proton source.[29] The effect of various proton sources on the Fe(dophen) system was also investigated. The cyclic voltammogram of **2** under CO_2 and in the presence of 0.32 M CF_3CH_2OH is also depicted in Fig. 6. The cathodic current rises sharply beyond −2.0 V, indicating that the presence of CF_3CH_2OH enhances the rate of the catalytic reduction process. Enhancement in cathodic current is also observed for methanol but the effect is smaller. No such current enhancement can be observed if only alcohol but no CO_2 is present; hence the increase in cathodic current cannot be due to the direct reduction of alcohol by the Fe(I) complex. When protonated amines such as $(CH_3)_3NH^+$, $(CH_3)_2NH_2^+$ or $(C_2H_5)_3NH^+$ are used as the proton source, an increase in cathodic current is observed even when CO_2 is absent, indicating that the Fe(I) species catalyzes the direct reduction of these protic species. The same effects were observed for **1** under similar experimental conditions. The effect of water on the catalytic properties of **1** and **2** could not be tested because water causes precipitation of the iron complexes.

The results of constant potential electrolysis of CO_2 at a reticulated vitreous carbon working electrode under various conditions with **1** or **2** as catalyst are summarized in Table 4. The product distribution obtained from bulk electrolysis is independent of whether DMSO or DMF is used as the solvent. It is noted that formate is the major product formed in the absence of any added proton source. When anhydrous $LiClO_4$ is used as the supporting electrolyte instead of TBAH, the same amount of formate is obtained. Therefore, the protons responsible for the production of formate should have originated from the solvent or trace of water present in the electrolyte; the possibility that TBAH acts as the proton source can be ruled out. Addition of alcohol to the electrolyte increases the rate of reaction and promotes the production of carbon monoxide. For example, the addition of 1.23 M CF_3CH_2OH to the electrolyte (0.1 M TBAH in DMSO) increases the percentage yield of CO from 18.5% to 29.5% with **2** as the catalyst (Table 4). As in the other systems,[11e,12b] the presence of alcohol can slow down the degradation of catalyst in the course of the reaction: the decay of **2** per catalytic cycle is 4% with trifluoroethanol and 7% with methanol, whereas in the absence of alcohol it is 13%. When $(CH_3)_3NH^+$, $(CH_3)_2NH_2^+$ or $(C_2H_5)_3NH^+$ is used as the proton source, dihydrogen gas is the major product though a small amount of CO is also produced.

In-situ FTIR spectroelectrochemical studies

DMSO is preferred over DMF in performing *in-situ* FTIR spectroelectrochemical experiments because the latter absorbs strongly in the 1600–1400 cm^{-1} region. As the same catalytic mechanism is expected to operate for **1** and **2**, *in-situ* FTIR spectroelectrochemical studies were only conducted on **2**. Fig. 7a reveals a series of normalized time-resolved FTIR spectra in the 3500–1750 cm^{-1} region obtained with a glassy carbon working electrode in a DMSO solution of **2** saturated with CO_2. The reference (E_1) and the working (E_2) potential of the glassy carbon electrode were held at −0.46 V and −2.16 V *vs.* $Cp_2Fe^{+/0}$ respectively. The spectra collected at E_2 at different time intervals were normalized to the reference spectrum taken at E_1.

The spectra reveal an intense growth of features in the region 3200–3000 cm^{-1} upon stepping the potential to −2.16 V. Based on previous investigations,[20,30] these bands can be assigned to the accumulation of tetrabutylammonium cations (TBA^+) at the thin layer when the working electrode potential is increased towards the cathodic side. The positive band at 2343 cm^{-1} is attributed to the consumption of CO_2 during the course of reduction. In addition, a small negative band appears at 2140 cm^{-1}, which is most appropriately assigned to the presence of CO.[31] The low intensity of the CO absorption band is due to the molecule's weak oscillator strength (eight times less than CO_2)[31] and its low solubility in DMSO (solubility = 130 mM at 25 °C).[32]

The spectra also reveal that a species with absorption peaks at 1934 cm^{-1} and 1881 cm^{-1} was generated during the course of reduction (Fig. 7a). This species was formed prior to the release of free CO. The intensity of these two bands became constant in the later course of the reduction process. Previous study by Christensen *et al.*[30b] indicates that metal dicarbonyl species absorb in this region. Thus, it is reasonable to assign these features to the presence of an iron carbonyl (Fe–CO) species. In addition, a negative band at 1328 cm^{-1} was observed, which can be attributed to the formation of an iron formato intermediate (Fe–OC(O)H) during the course of reduction (Fig. 7b). The above assignments are supported by $^{13}CO_2$ isotope experiments: a positive band corresponding to the consumption of $^{13}CO_2$ (2278 cm^{-1}) and negative bands attributable to the formation of ^{13}CO (2110 cm^{-1}), Fe–^{13}CO (1867, 1814 cm^{-1}) and Fe–$O^{13}C(O)H$ (1288 cm^{-1}) were observed. In the presence of 1.23 M CF_3CH_2OH, the spectra (Fig. S2 in the supplementary information) show similar bands attributable to the presence of Fe–CO (ν = 1932 cm^{-1}, 1879 cm^{-1}) and Fe–OC(O)H species (ν = 1326 cm^{-1}). The spectral changes are very similar to those obtained in the absence of CF_3CH_2OH. This may be because the same intermediates are involved under both conditions.

Mechanism of CO_2 reduction

The reaction mechanism of CO_2 reduction by the iron complexes in the present study is complicated, as a mixture of CO, $HCOO^-$ and $C_2O_4^{2-}$ is produced. This also precludes the use of simple electrochemical kinetic models for mechanistic investigation. To date, the formation of CO is generally accepted to occur *via* a M–η^1-CO_2 intermediate. For example, the reduction of CO_2 to CO by nickel cyclam catalysts occurs with nearly 100% current efficiency in water at pH 4.1; the high selectivity is attributed to the formation of a Ni–η^1-CO_2 intermediate which is stabilized by hydrogen bonding between the carbon dioxide oxygen and the secondary amine hydrogen of the cyclam ligand.[9d,33] The formation of the M–η^1-CO_2 complex is favoured by the charge-transfer interaction from the d_{z^2} orbital of an electron-rich metal center to the π* orbital of CO_2.[34] This was exemplified by the work of Tanaka *et al.*[35] and Deronzier

Table 4 A summary on the electrolysis of CO_2 in the presence of **1** or **2**

Solvent	Proton source[c]	Charge consumed/C	Current efficiency of CO produced/%	Current efficiency of $HCOO^-$ produced/%	Current efficiency of $C_2O_4^{2-}$ produced/%	Current efficiency of H_2 produced/%
DMSO[a]	—	3.29 (3.08)[d]	18.5 (23.9)[d]	67.2 (66.8)[d]	9.8 (7.8)[d]	—
DMSO[a]	1.23 M CF_3CH_2OH	10.47	29.5	65.4	2.9	—
DMSO[a]	1.23 M CH_3OH	8.01 (5.90)[e]	25.8 (—)[e]	66.4 (—)[e]	6.4 (—)[e]	— (40.6)[e]
DMSO[a]	0.16 M $(CH_3)_3NH^+Cl^-$	14.71	10.5	—	—	69.5
DMSO[a]	0.16 M $(CH_3)_2NH_2^+Cl^-$	13.31	9.8	—	—	78.5
DMSO[a]	0.16 M $(C_2H_5)_3NH^+Cl^-$	15.81	11.4	—	—	72.1
DMF[a]	—	9.98	22.5	57.2	13.4	—
DMF[a]	1.23 M CH_3OH	7.63	29.8	51.5	10.6	—
DMF[a]	1.23 M CF_3CH_2OH	8.73 (7.83)[e]	31.2 (—)[e]	52.6 (—)[e]	8.5 (—)[e]	— (47.6)[e]
DMF[b]	—	10.93	23.9	58.9	11.1	—
DMF[b]	1.23M CF_3CH_2OH	8.30	42.4	46.4	3.0	—
DMSO[b]	—	6.88	13.3	73.6	7.3	—
DMSO[b]	1.23 M CF_3CH_2OH	8.03	25.5	63.9	4.7	—

[a] **2** (1×10^{-3} M) as catalyst; electrolysis time: 1 h; potential held at −2.0 V *vs.* $Cp_2Fe^{+/0}$; supporting electrolyte: 0.1 M TBAH. [b] **1** (5×10^{-4} M) as catalyst; electrolysis time: 1 h; potential held at −2.0 V *vs.* $Cp_2Fe^{+/0}$; supporting electrolyte: 0.1 M TBAH. [c] The concentration of proton source that gives the maximum current in the cyclic voltammogram was chosen in the electrolysis. [d] 0.1 M $LiClO_4$ was used as the supporting electrolyte. [e] Electrolysis conducted in N_2-saturated DMSO; electrolysis time: 2 h.

et al.,[36] who demonstrated that electron-donating groups on the 4, 4′ positions of the bipyridyl ligands of ruthenium bipyridyl carbonyl catalysts can promote the selective formation of CO in aqueous medium. It is believed that the electron-donating groups increase the electron density of the metal center thus favouring the formation of a Ru–η^1-CO_2 intermediate. The proposed formation of an Fe–η^1-CO_2 complex between Fe(I) and CO_2 is shown in Scheme 1.

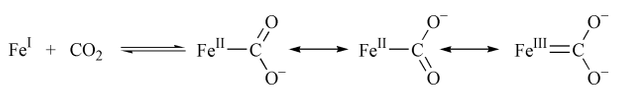

Scheme 1

Upon charge transfer from Fe^I to CO_2, the electron density increases around the CO_2 oxygen atoms. As a result, the coordinated CO_2 is activated to electrophilic attack.[34] In the palladium phosphine catalysts studied by DuBois *et al.*, CO_2 is reduced to CO in DMF with current efficiencies greater than 95% in the presence of 0.02 M HBF_4.[8b] Savéant and co-workers have reported that addition of weak proton sources such as 2,2,2-trifluoroethanol enhances the rate of iron-porphyrin catalyzed reduction of CO_2 to CO with current efficiencies close to 100%.[12b] For the rhenium bipyridyl carbonyl catalysts, addition of water enhances the catalytic rate and improves the selectivity of CO formation[11a,e]. Weak Brönsted acids can stabilize the M–η^1-CO_2 complex by serving as an electron sink through hydrogen bond formation with the carbon dioxide oxygens.[12b,37] Under such conditions, the charge transfer from the metal center to the coordinated CO_2 becomes more facile and the CO_2 moiety is further activated.[38] This facilitates the cleavage of a C–O bond leading to the formation of a M–CO intermediate, which will subsequently release the carbonyl ligand as CO. This mechanism is supported by the appearance of absorption bands assignable to an iron carbonyl intermediate in the time resolved infrared spectra and the observation that CO was formed at the expense of the Fe–CO species. The proposed mechanism for CO formation in the Fe(dophen) system is shown in Scheme 2 below.

In the Fe(dophen) system, oxalate is obtained as a minor product whether in the absence of added proton source or in the presence of alcohol. The formation of oxalate is usually attributed to the dimerization of two reduced CO_2 molecules.[39] Presumably, dissociation of the reduced CO_2 from the metal center produces $CO_2^{\bullet-}$, which will undergo dimerization to give $C_2O_4^{2-}$ (Scheme 3). Early dissociation of reduced CO_2 would occur more readily in M–η^1-CO_2 complexes in which the metal

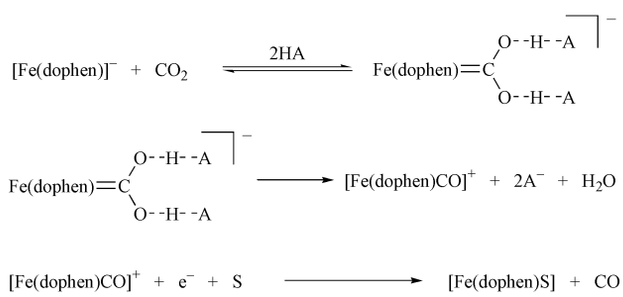

Scheme 2 S is a solvent molecule.

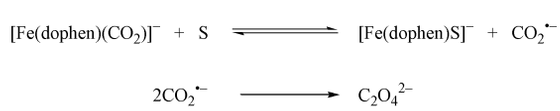

Scheme 3

centers are not sufficiently electron rich and hence the M–C bonds are relatively weak.

It is interesting to note that formate is obtained as the major product in [Fe(dophen)] catalyzed CO_2 reduction except when protonated amines are present as the proton source (Table 4). This is in contrast to the iron porphyrin catalyst, which selectively gives CO as the major product.[12b] There are controversies over the mechanism of formate production in the literature: metal hydride (M–H),[36] metal formyl (M–CHO),[40] metal carboxylate (M–COOH)[35] and metal formato (M–OCHO)[41] species have all been proposed as the intermediate. Selective formation of $HCOO^-$ has been reported for the $[Ru(bpy)(CO)_2]^{2+}$ catalyst (bpy = 2,2′-bipyridine) in the presence of protonated amine.[29] A number of metal hydride catalysts are also known to produce $HCOO^-$ selectively.[10d,41] Deronzier *et al.* reported that placing electron-withdrawing substituents on the 4,4′ position of L in $[Ru(L)(CO)_2]_n$ (L = bipypyridyl ligand) would change the CO/$HCOO^-$ selectivity drastically and lead to the quantitative production of $HCOO^-$.[36] They attributed this finding to the decrease in the electron density of the metal center, which makes the formation of M–η^1-CO_2 less favorable. *Ab initio* MO calculations also support that the C coordination mode (M–CO_2) is not favourable if the electron density on the metal ion is relatively low.[42] The formal oxidation state of the active iron porphyrin catalyst is Fe(0).[12b] Presumably, the Fe(0) center in the porphyrin system is more electron rich than the Fe(I) species in the present study, and the formation of Fe–η^1-CO_2 (and hence CO) is less favourable in the latter. It is noted that in the

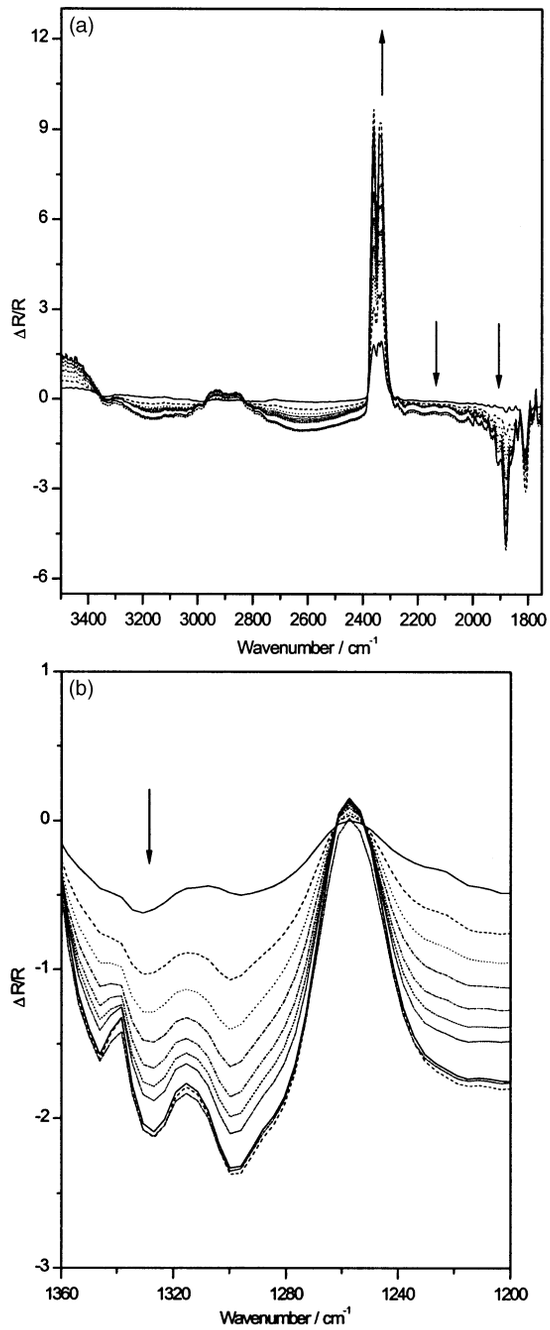

Fig. 7 (a) Normalized time resolved FTIR spectra in the region 3500–1750 cm^{-1} (8 cm^{-1} resolution, 100 scans) collected from a glassy carbon working electrode in a DMSO solution of **2** (5 mM) saturated with CO_2. E_2 = −2.16 V and E_1 = −0.46 V *vs.* $Cp_2Fe^{+/0}$. Supporting electrolyte: 0.1 M TBAH. Consecutive spectra were recorded at 45s intervals. (b) Expanded spectra of (a) in the region 1360–1200 cm^{-1}.

presence of the relatively strong Brönsted acids $(CH_3)_3NH^+$, $(CH_3)_2NH_2^+$ and $(C_2H_5)_3NH^+$ (pK_a in DMSO = 8.4, 10.3 and 9.0 respectively[43]), dihydrogen is produced as the major product though a small quantity of CO is also produced (Table 4). In the absence of CO_2, electrolysis of CF_3CH_2OH (pK_a 23.45)[43] or CH_3OH (pK_a 29.0)[43] in the presence of the iron catalysts also produced a substantial amount of hydrogen gas. Metal–hydride species formed by the reaction between reduced metals and Brönsted acids are well known for H_2 production.[44] If the reduced iron catalyst reacts with protons to form a hydride complex, subsequent insertion of CO_2 into the Fe–H species will lead to the production of $HCOO^-$.[45] The CO_2 molecule will compete with the proton source in the electrolyte for the Fe–H species. A weak Brönsted acid would favour the formation of $HCOO^-$ whereas a strong Brönsted acid would lead to the production of H_2. Attempts were made to detect Fe–H species in the time-resolved infrared spectra. However, no signs of Fe–H can be traced from the spectroscopic data at room temperature. The Fe–H species, being an early transition metal hydride, is expected to be a very reactive species.[46] Attempts to detect the Fe–H species at low temperatures were limited by the high melting point of DMSO (18.4 °C) which causes the electrolyte to solidify rapidly as the temperature is lowered. We are in favour of an Fe–H but not an Fe–COOH intermediate for $HCOO^-$ production for the following reasons: (i) electrolysis of the proton sources with the iron catalyst in the absence of CO_2 produced a substantial amount of hydrogen gas (Table 4), which supports the formation of an Fe–H species; (ii) in the electrolysis of CO_2 with protonated amine, only CO and H_2 but no $HCOO^-$ were obtained. If $HCOO^-$ were originated from an Fe–COOH intermediate, we would expect formate to be formed concomitantly with carbon monoxide; (iii) in a recent study in our laboratory on the reduction of CO_2 to $HCOO^-$ by a ruthenium carbonyl catalyst in the presence of different proton sources in acetonitrile, a Ru–H species was detected by *in-situ* FTIR spectroelectrochemistry at −0.5 °C.[47] Scheme 4 shows our postulated mechanism for $HCOO^-$ production.

$$[Fe(dophen)]^- + AH \rightleftharpoons [Fe(dophen)H] + A^-$$

$$[Fe(dophen)H] + CO_2 \rightleftharpoons [Fe(dophen)OC(O)H]$$

$$[Fe(dophen)OC(O)H] + e^- + S \longrightarrow [Fe(dophen)S] + HCOO^-$$

Scheme 4 S is a solvent molecule.

Conclusion

Two iron complexes of 2,9-bis(2-hydroxyphenyl)-1,10-phenanthroline, **1** and **2**, have been synthesized and their X-ray crystal structures have been solved. Both complexes are catalysts for the electroreduction of CO_2; the active catalyst is an iron(I) species. The rate of CO_2 reduction is enhanced by the addition of alcohol as the proton source. The result of *in-situ* FTIR spectroelectrochemical study reveals that an iron carbonyl and an iron formato species are involved in the reduction process. The formation of CO and $HCOO^-$ are postulated to occur *via* two competing pathways.

Acknowledgements

The financial support from the Hong Kong Polytechnic University (K. Y. W.) and the University of Hong Kong (C. M. C.) are gratefully acknowledged. S. N. P. acknowledges the award of a tuition scholarship by the Research Committee of the Hong Kong Polytechnic University and a fellowship by the Sir Edward Youde memorial fund.

References

1 (*a*) E. Monnin, A. Indermühle, A. Dällenbach, J. Flückiger, B. Stauffer, T. F. Stocker, D. Raynaud and J.-M. Barnola, *Science*, 2001, **291**, 112; (*b*) D. Schoen, *Environ. Sci. Tech.*, 1999, **33**, 160A.
2 B. P. Sullivan, K. Krist and H. E. Guard (editors), *Electrochemical and Electrocatalytic Reactions of Carbon Dioxide*, Elsevier, Amsterdam, 1993.
3 W. Leitner, *Angew. Chem., Int. Ed. Engl.*, 1995, **34**, 2207.
4 J. P. Collin and J. P. Sauvage, *Coord. Chem. Rev.*, 1989, **93**, 245.
5 K. Tanaka, in *Advances in Inorganic Chemistry*, ed. A. G. Skyes, Academic Press, New York, 1995, vol. 43, pp. 409–435.
6 I. Taniguchi, in *Modern Aspects of Electrochemistry*, eds. J. O'M. Bockris, R. E. White and B. E. Conway, Plenum Press, New York, 1989, vol. 20, ch. 5.
7 (*a*) S. Meshitsuka, M. Ichikawa and K. Tamaru, *J. Chem. Soc., Chem. Commun.*, 1974, 158; (*b*) K. Takahashi, K. Hiratsuka, H. Sasaki and S. Toshima, *Chem. Lett.*, 1979, 305; (*c*) S. Kapusta

and N. Hackerman, *J. Electrochem. Soc.*, 1984, **131**, 1511; (*d*) C. M. Lieber and N. S. Lewis, *J. Am. Chem. Soc.*, 1984, **106**, 5033; (*e*) J. Y. Becker, B. Vainas, R. Eger and L. Kaufman, *J. Chem. Soc., Chem. Commun.*, 1985, 1471; (*f*) T. Atoguchi, A. Aramata, A. Kazusaka and M. Enyo, *J. Chem. Soc., Chem. Commun.*, 1991, 156; (*g*) T. Yoshida, K. Kamato, M. Tsukamoto, T. Iida, D. Schlettwein, D. Wöhrle and M. Kaneko, *J. Electroanal. Chem.*, 1995, **385**, 209.

8 (*a*) D. L. DuBois and A. Miedaner, *J. Am. Chem. Soc.*, 1987, **109**, 113; (*b*) D. L. DuBois, A. Miedaner and R. C. Haltiwanger, *J. Am. Chem. Soc.*, 1991, **113**, 8753; (*c*) A. Miedaner, C. J. Curtis, R. M. Barkley and D. L. DuBois, *Inorg. Chem.*, 1994, **33**, 5482; (*d*) B. D. Steffey, C. J. Curtis and D. L. DuBois, *Organometallics*, 1995, **14**, 4937; (*e*) A. L. Miedaner, B. C. Noll and D. L. DuBois, *Organometallics*, 1997, **16**, 5779.

9 (*a*) J. Costamagna, G. Ferraudi, J. Canales and J. Vargas, *Coord. Chem. Rev.*, 1996, **148**, 221; (*b*) D. J. Darensbourg and M. W. Holtcap, *Coord. Chem. Rev.*, 1996, **153**, 155, and references therein; (*c*) B. Fisher and R. Eisenberg, *J. Am. Chem. Soc.*, 1980, **102**, 7361; (*d*) M. Beley, J.-P. Collin, R. Ruppert and J.-P. Sauvage, *J. Am. Chem. Soc.*, 1986, **108**, 7461; (*e*) G. B. Balazs and F. C. Anson, *J. Electroanal. Chem.*, 1992, **322**, 325; (*f*) E. Fujita, J. Haff, R. Sanzenbacher and H. Elias, *Inorg. Chem.*, 1994, **33**, 4627.

10 (*a*) H. Ishida, K. Tanaka and T. Tanaka, *Organometallics*, 1987, **6**, 181; (*b*) H. Nagao, T. Mizukawa and K. Tanaka, *Inorg. Chem.*, 1994, **33**, 3415; (*c*) M. M. Ali, H. Sato, T. Mizukawa, K. Tsuge, M. Haga and K. Tanaka, *Chem. Commun.*, 1998, 249; (*d*) J. R. Pugh, M. R. M. Bruce, B. P. Sullivan and T. J. Meyer, *Inorg. Chem.*, 1991, **30**, 86; (*e*) M.-N. Collomb-Dunand-Sauthier, A. Deronzier and R. Ziessel, *Inorg. Chem.*, 1994, **33**, 2961; (*f*) S. Chardon-Noblat, A. Deronzier, R. Ziessel and D. Zsoldos, *Inorg. Chem.*, 1997, **36**, 5384.

11 (*a*) J. Hawecker, J.-M. Lehn and R. Ziessel, *J. Chem. Soc., Chem. Commun.*, 1984, 328; (*b*) B. P. Sullivan, C. M. Bolinger, D. Conrad, W. J. Vining and T. J. Meyer, *J. Chem. Soc., Chem. Commun.*, 1985, 1414; (*c*) T. Yoshida, K. Tsutsumida, S. Teratani, K. Yasufuku and M. Kaneko, *J. Chem. Soc., Chem. Commun.*, 1993, 631; (*d*) S. Cosnier, A. Deronzier and J.-C. Moutet, *New. J. Chem.*, 1990, **14**, 831; (*e*) K. Y. Wong, W. H. Chung and C. P. Lau, *J. Electroanal. Chem.*, 1998, **453**, 161.

12 (*a*) M. Hammouche, D. Lexa and J.-M. Savéant, *J. Am. Chem. Soc.*, 1991, **113**, 8455; (*b*) I. Bhugun, D. Lexa and J.-M. Savéant, *J. Am. Chem. Soc.*, 1996, **118**, 1769.

13 C. Bernard, Y. LeMest and J. P. Gisselbrecht, *Inorg. Chem.*, 1998, **37**, 181.

14 (*a*) K. Ogura, N. Endo, M. Nakayama and H. Ootsuka, *J. Electrochem. Soc.*, 1995, **142**, 4026; (*b*) K. Ogura, M. Nakayama and C. Kusumoto, *J. Electrochem. Soc.*, 1996, **143**, 3606; (*c*) M. Nakayama, M. Iino and K. Ogura, *J. Electroanal. Chem.*, 1997, **440**, 251.

15 (*a*) C. Arana, S. Yan, M. Keshavarz-K, K. T. Potts and H. D. Abruña, *Inorg. Chem.*, 1992, **31**, 3680; (*b*) J. A. Ramos Sende, C. R. Arana, L. Hernández, K. T. Potts, M. Keshavarz-K and H. D. Abruña, *Inorg. Chem.*, 1995, **34**, 3339.

16 P. Capdevielle, M. Maumy and P. Audebert, *New. J. Chem.*, 1994, **18**, 519.

17 W. H. Chung, P. Guo, K. Y. Wong and C. P. Lau, *J. Electroanal. Chem.*, 2000, **486**, 32.

18 M. A. Masood and P. S. Zacharias, *J. Chem. Soc., Dalton Trans.*, 1991, 111.

19 A. J. Bard and L. R. Faulkner, *Electrochemical Methods, Fundamentals and Applications*, Wiley, New York, 1980, p. 701.

20 P. A. Christensen, A. Hamnett and J. A. Timney, *J. Chem. Soc., Dalton Trans.*, 1992, 1455.

21 S. G. Sun, D. F. Yang and Z. W. Tian, *J. Electroanal. Chem.*, 1990, **289**, 177.

22 E. J. Gabe, Y. Le Page, J. P. Charland, F. L. Lee and P. S. White, *J. Appl. Crystallogr.*, 1989, **22**, 384.

23 M. Gerloch and F. E. Mabbs, *J. Chem. Soc. A*, 1967, 1900.

24 J. Baker, L. M. Engelhardt, B. M. Figgis and A. H. White, *J. Chem. Soc., Dalton Trans.*, 1975, 530.

25 C. M. Che, W. H. Leung, C. K. Li, H. Y. Cheng and S. M. Peng, *Inorg. Chim. Acta*, 1992, **196**, 43.

26 G. Balducci, G. Chottard, D. Lexa and J.-M. Savéant, *Inorg. Chem.*, 1994, **33**, 1972.

27 D. G. Davis and L. A. Constant, *Anal. Chem.*, 1975, **47**, 2253.

28 (*a*) M. Gerloch, J. Lewis, F. E. Mabbs and A. Richards, *Nature (London)*, 1966, **212**, 809; (*b*) M. Gerloch and F. E. Mabbs, *J. Chem. Soc. A*, 1967, 1598; (*c*) S. E. Wenk and F. A. Schultz, *J. Electroanal. Chem.*, 1979, **101**, 89.

29 H. Ishida, H. Tanaka, K. Tanaka and T. Tanaka, *J. Chem. Soc., Chem. Commun.*, 1987, 131.

30 (*a*) P. A. Christensen and S. J. Higgins, *J. Electroanal. Chem.*, 1995, **387**, 127; (*b*) P. A. Christensen, A. Hamnett, J. A. Timney and S. J. Higgins, *J. Electroanal. Chem.*, 1995, **395**, 195.

31 F. Hartl, G. J. Stor and D. J. Stufkens, *Organometallics*, 1995, **14**, 1115.

32 I. Bhugun, D. Lexa and S.-M. Savéant, *Anal. Chem.*, 1994, **66**, 3994.

33 E. Fujita, C. Creutz, N. Sutin and B. S. Brunschwig, *Inorg. Chem.*, 1993, **32**, 2657.

34 D. H. Gibson, *Chem. Rev.*, 1996, **96**, 2063.

35 H. Ishida, K. Fujiki, T. Ohba, K. Ohkubo, K. Tanaka, T. Terada and T. Tanaka, *J. Chem. Soc., Dalton Trans.*, 1990, 2155.

36 S. Chardon-Noblat, A. Deronzier, R. Ziessel and D. Zsoldos, *J. Electroanal. Chem.*, 1998, **444**, 253.

37 H. Tanaka, B.-C. Tzeng, H. Nagao, S.-M. Peng and K. Tanaka, *Inorg. Chem.*, 1993, **32**, 1508.

38 S. Sakaki, *J. Am. Chem. Soc.*, 1992, **114**, 2055.

39 (*a*) A. Gennaro, A. A. Isse, J.-M. Savéant, M.-G. Severin and E. Vianello, *J. Am. Chem. Soc.*, 1996, **118**, 7190; (*b*) K. Tanaka, Y. Kushi, K. Tsuge, K. Toyohara, T. Nishioka and K. Isobe, *Inorg. Chem.*, 1998, **37**, 120.

40 K. Toyohara, H. Nagao, T. Mizukawa and K. Tanaka, *Inorg. Chem.*, 1995, **34**, 5399.

41 J. R. Pugh, M. R. M. Bruce, P. B. Sullivan and T. J. Meyer, *Inorg. Chem.*, 1991, **30**, 86.

42 S. Sakaki, K. Kitaura and K. Morokuma, *Inorg. Chem.*, 1982, **21**, 760.

43 K. Izutsu, *Acid-base Dissociation Constants in Dipolar Aprotic Solvents*, Blackwell Scientific Publications, Oxford, 1990.

44 (*a*) J.-M. Savéant, I. Bhugun and D. Lexa, *J. Am. Chem. Soc.*, 1996, **118**, 3982; (*b*) J.-M. Savéant, V. Grass and D. Lexa, *J. Am. Chem. Soc.*, 1997, **119**, 7526; (*c*) J. P. Collman, Y. Ha, P. S. Wagenknecht, M. A. Lopez and R. Guilard, *J. Am. Chem. Soc.*, 1993, **115**, 9080; (*d*) J. P. Collman, P. S. Wagenknecht and N. S. Lewis, *J. Am. Chem. Soc.*, 1992, **114**, 5665.

45 L. D. Field, E. T. Lawrenz, W. J. Shaw and P. Turner, *Inorg. Chem.*, 2000, **39**, 5632.

46 S. S. Kristjansdottir and J. R. Norton, in *Transition Metal Hydrides*, ed. A. Dedien, VCH, New York, 1992, ch. 9.

47 S. N. Pun and K. Y. Wong, unpublished work.